JCTC Journal of Chemical Theory and Computation

ARTICLE

pubs.acs.org/JCTC

Prediction of Charge Mobility in Amorphous Organic Materials through the Application of Hopping Theory

Choongkeun Lee,[†] Robert Waterland,[‡] and Karl Sohlberg*[,†]

[†]Department of Chemistry, Drexel University, Philadelphia, Pennsylvania 19104-2875, United States

[‡]Central Research and Development, E. I. du Pont de Nemours & Co., Inc., Wilmington, Delaware 19880-0320, United States

ABSTRACT: The application of hopping theory to predict charge (hole) mobility in amorphous organic molecular materials is studied in detail. Application is made to amorphous cells of *N*,*N*′-diphenyl-*N*,*N*′-*bis*-(3-methylphenylene)-1,1′-diphenyl-4,4′-diamine (TPD), 1,1-*bis*-(4,4′-diethylaminophenyl)-4,4-diphenyl-1,3,butadinene (DEPB), *N*4,*N*4′-di(biphenyl-3-yl)-*N*4,*N*4′-diphenylbiphenyl-4,4′-diamine (mBPD), *N*1,*N*4-di(naphthalen-1-yl)-*N*1,*N*4-diphenylbenzene-1,4-diamine (NNP), and *N*,*N*′-bis-[9,9-dimethyl-2-fluorenyl]-*N*,*N*′-diphenyl-9,9-dimethylfluorene-2,7-diamine (pFFA). Detailed analysis of the computation of each of the parameters in the equations for hopping rate is presented, including studies of their convergence with respect to various numerical approximations. Based on these convergence studies, the most robust methodology is then applied to investigate the dependence of mobility on such parameters as the monomer reorganization energy, the monomer−monomer coupling, and the material density. The results give insight into what will be required to improve the accuracy of predictions of mobility in amorphous organic materials, and what factors should be controlled to develop materials with higher (or lower) charge (hole) mobility.

1. INTRODUCTION

Organic conducting materials are receiving significant scrutiny for possible application in the development of lightweight, cheap, and flexible electronic devices, such as organic light-emitting diodes (OLED), data storage systems, field-effect transistors (FET), or solar cells.[1−3] While organic conductors have numerous advantages over established technology, the hole mobility of most organic crystals ($\sim 10^{-2}$ cm^2/V s) is much smaller than that of the inorganic materials in common use. Recently, however, organic crystals, such as pentacene and phthalocyanine, have been produced with improved conducting properties, thereby invigorating the field. The mobility of pentacene has been improved from 2×10^{-3} to 1.5 cm^2/V s and that of phthalocyanine from 10^{-3} to 0.02 cm^2/V s using improved fabrication technology.[4]

Some characteristics of high-performance organic electronic materials are well established. For example, discotic liquid crystal molecules that have one or more strong resonance rings at their center often show good charge mobility. This results from a low reorganization energy and a large electronic splitting.[5−10] The strong resonance ring tends to make the molecules form columnar phases, leading to a pseudo-one-dimensional charge-transfer pathway. Such a one-dimensional charge-transfer path was observed in our previous work on phthalocyanine, in which we showed that the coupling matrix element is high only for the face to face charge-transfer dimer.[11] For this face to face charge transfer, the site energies are nearly identical, producing very low energetic disorder. The large coupling matrix element and the low energetic disorder combine to yield high charge mobility.

Although the mechanism of charge transfer in organic crystals has been studied for several decades, the capability to predict charge mobility in amorphous materials is still very limited. Tse and colleagues have reviewed three general approaches to modeling charge transport.[12] Historically, charge transport was modeled with macroscopic phenomenological models. The currently most popular approach is to employ the Gaussian disorder model (GDM). The GDM approach, which is most appropriate when charge transport is dominated by energetic disorder in the hopping sites,[13] was developed by Bässler and colleagues[14−16] and used extensively by others.[17,18] The third approach, and the one adopted for the present work, is to apply Marcus hopping theory, which is especially useful when polaron effects are significant.[13] In amorphous organic materials, charge mobility cannot be predicted by simple application of Marcus−Hush theory, however, because all molecules are inequivalent due spatial disorder, so energetic disorder in the matrix cannot be disregarded.[19−21] To predict the charge mobility adequately, the site energy must be reliably incorporated.

We seek to identify a reliable and computationally efficient computational method for screening amorphous molecular solids for high hole mobility. Toward this end, in this study we explore the application of hopping theory to calculate charge (hole) mobility in amorphous *N*,*N*′-diphenyl-*N*,*N*′-*bis*-(3-methylphenylene)-1,1′-diphenyl-4,4′-diamine (TPD), 1,1-*bis*-(4,4′-diethylaminophenyl)-4,4-diphenyl-1,3,butadinene (DEPB), *N*4,*N*4′-di(biphenyl-3-yl)-*N*4,*N*4′-diphenylbiphenyl-4,4′-diamine (mBPD), *N*1,*N*4-di(naphthalen-1-yl)-*N*1,*N*4-diphenylbenzene-1,4-diamine (NNP), and *N*,*N*′-bis[9,9-dimethyl-2-fluorenyl]-*N*,*N*′-diphenyl-9,9-dimethylfluorene-2,7-diamine (pFFA) (for which the chemical structures are shown in Figure 1). For comparison, we also calculate charge (hole) mobility in crystalline tetracene and pentacene. First, we describe the theoretical/computational approach. Next, we report detailed studies of the various approximations employed. Finally, numerous factors controlling the mobility are investigated, including the influence of the

Received: May 21, 2011
Published: June 29, 2011

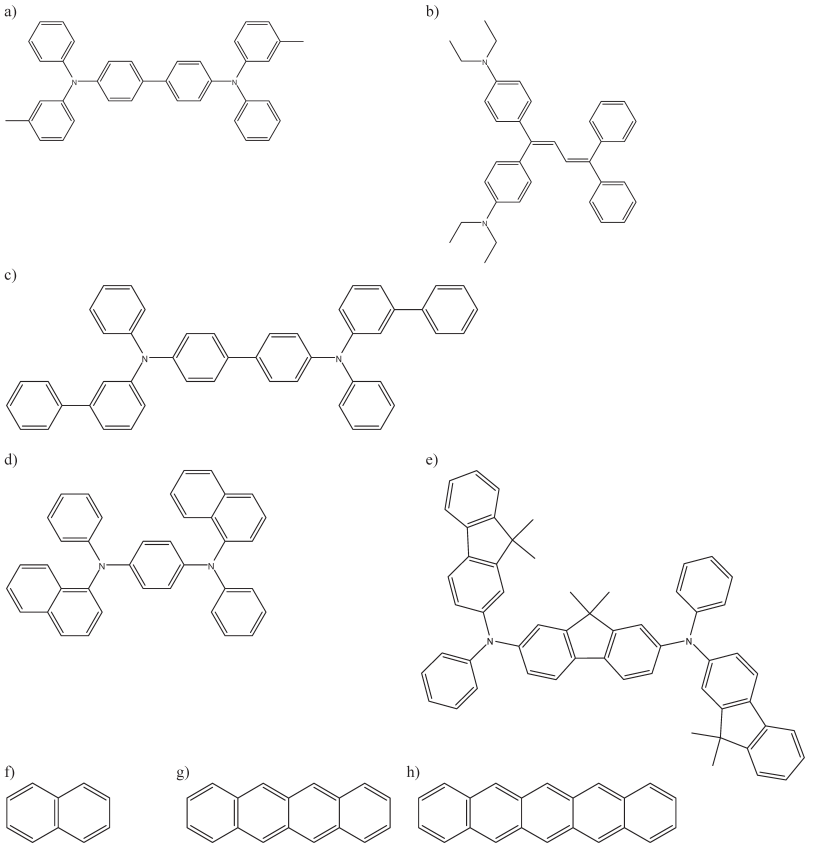

Figure 1. Chemical structures of the monomers of the amorphous materials studied here: (a) TPD, (b) DEPB, (c) mBPD, (d) NNP, (e) pFFA, (f) naphthalene, (g) tetracene, and (h) pentacene.

dielectric properties of the material matrix on the reorganization energy, the dependence of charge mobility on material density, and the method of treating site energy.

2. THEORY AND COMPUTATIONAL METHODS

2.1. Overview. Our approach to computing charge mobility in amorphous molecular solids is based on modeling the following fundamental step in the charge-transport process. If "M" represents the basic monomer unit of the material, (a single molecule) we consider the rate of hopping of a charge between one monomer and an adjacent one:

$$M^+ + M \rightarrow M + M^+ \quad (1)$$

in the presence of a disordered background distribution of M. The disordered background distribution represents the material bulk.

To model the material bulk, we construct an ensemble of representative unit cells, using a procedure described in detail in Section 2.2. These unit cells are constructed to be sufficiently large so that for a representative monomer near the center of the cell, the nearest-neighbor interactions involve other monomers within the same cell. We refer to these cells as "amorphous cells", while acknowledging that a material built by translational repetition of such a cell would have periodicity on the length scale of the cell dimension.

Next, for each cell, hopping theory is applied to a selected monomer within the cell to compute the rate of charge hopping to the adjacent monomers. These hopping rates are then combined to determine a hole mobility for the cell. The ensemble of cells therefore gives rise to a distribution of mobility values, and the average value of mobility over the entire ensemble is taken as the estimate of mobility in the material. This approach, outlined above and detailed in the balance of this paper, explicitly incorporates energetic disorder of the sites in the material and does so without the introduction of an adjustable "disorder parameter" common to simulation approaches to computing mobility.[22−24] The use of an explicit cell model also avoids the severe assumption of isotropic monomer−monomer interactions. Instead, each such interaction is treated explicitly.

2.2. Construction of Amorphous Cells. Amorphous cell representations of TPD, DEPB, mBPD, NNP, and pFFA were generated using the amorphous cell construction and forcite modules of Accelrys' Materials Studio 5.0 commercial code.[25] There are no material density measurements for any of the amorphous organic materials studied in this paper. Since the charge mobility depends exponentially on density (vide infra), we first accurately determined material densities using the procedure developed by Rigby.[26] In brief, the molecular monomer structures shown in Figure 1a−e were first optimized using molecular mechanics and the COMPASS force field.[26] Ten cubic lattice amorphous cells were prepared for each material. Each cell was filled with sufficient copies of the optimized monomer structures to result in approximately 1600 atoms/cell. The starting cubic cell parameter was selected to make the density close to 1 g/cm^3, and the cells were energy minimized after generation. Each cell was subjected to four sequential forcite molecular dynamics runs: (i) a constant volume and temperature (NVT)

Table 1. X-ray Crystal Cell Parameters for Tetracene and Pentacene

	space group	*a* (Å)	*b* (Å)	*c* (Å)	α	*β*	*γ*
tetracene	$P\bar{1}$	7.98	6.14	13.57	101.3	113.2	87.5
pentacene	$P\bar{1}$	6.28	7.79	14.56	76.4	87.6	84.7

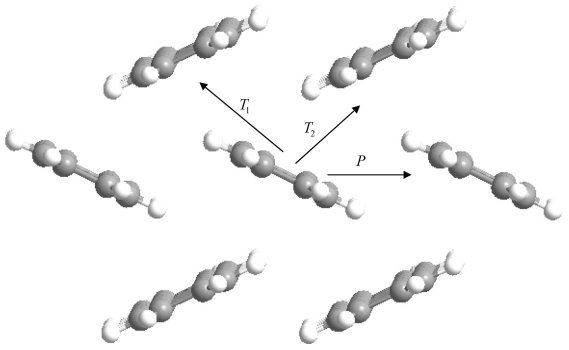

Figure 2. Neighbor interactions (P, T1, and T2) in the tetracene crystal.

velocity scaled run of 10 000 steps; (ii) a NVT run of 40 000 steps using the Andersen thermostat; (iii) a constant pressure and temperature (NPT) run of 10 000 steps; and (iv) a final production NPT run of 100 000 steps. Both NPT runs employed the Andersen and Berendsen thermostat and barostat and an applied external pressure of 0.0001 GPa. The time step for all of the dynamics runs was 1 fs. Full atomic coordinate frames were written out every 1000 steps of the production runs and used to compute the mean density and its standard deviation. The computed densities of TPD, DEPB, mBPD, NNP, and pFFA are 1.07, 1.01, 1.10, 1.14, and 1.02 ± 0.01 g/cm^3, respectively.

Subsequently these computed densities were used to generate more than 90 different amorphous cells for each material, each with ca. 20 molecules (24 and 15 molecules for NNP and pFFA, respectively) in the unit cell. Each generated cell was energy minimized to remove close contacts generated by the cell packing algorithm. These amorphous cells were generated in a cubic lattice, *a* = 26.9129, 26.6633, 26.8210, 26.1847, and 26.5138 Å for TPD, DEPB, mBPD, NNP, and pFFA, respectively.

The crystal structures of tetracene and pentacene were built up using X-ray diffraction data[27,28] with Material Studio.[25] Details of their structures are given in Table 1. In $P\bar{1}$ symmetry, there are 3 nearest-neighbor interactions, T1, T2, and P-type, and 1 long range interaction, L-type.[19,20] The three nearest neighbor interactions are displayed in Figure 2.

2.3. Mobility. To compute mobility for a given amorphous cell, we apply a generalization of Deng and Goddard's[19] implementation of Marcus−Hush theory.[29] In this approximation, mobility (μ) is given in terms of the charge diffusion coefficient *D*, unit charge *e*, temperature *T*, and Boltzmann constant k_B by an expression attributed to Einstein:

$$\mu = \frac{eD}{k_B T} \tag{2}$$

The diffusion coefficient is determined from a weighted average of the hole hopping rates W_{ij} from a representative monomer cation A_i^+ in the material to each of its interacting neutral neighbors A_j. The weight on each term is given by the product of the square of the distance to the neighbor r_{ij} and by the normalized hopping probability to the neighbor P_{ij}.

$$D = \frac{1}{2n}\sum_{i\neq j} r_{ij}^2 W_{ij} P_{ij} \tag{3}$$

The summation runs over all monomers within a cutoff radius r_c = 12 Å of the representative central molecule. (See Convergence Tests Section below.) The charge-hopping rate (without external electric field) is assumed to be given by the general expression:[19−21]

$$W_{ij} = \frac{{V_{ij}}^2}{\hbar}\left(\frac{\pi}{\lambda k_B T}\right)^{1/2} \exp\left(-\frac{(\Delta E_{ij} + \lambda)^2}{4\lambda k_B T}\right) \tag{4}$$

Where V_{ij} is the coupling matrix element, λ is the reorganization energy, $\hbar$ is Planck's constant, and ΔE_{ij} is the energy difference between the initial and final states in the hopping process. (This is nominally the energy difference between the reactants and the products in eq 1, which is, in general, not equal to zero because the presence of the disordered background removes the apparent symmetry of the reaction.) Note that throughout this work we make the implicit assumption that the free energy change for the hopping process (ΔG) is well approximated by the total energy change for the hopping process (ΔE_{ij}). This assumption is supported by the fact that the nuclear structures of the initial and final states are essentially the same in the crossing region,[30] so entropic considerations to both states are plausibly very similar. To apply eq 4 it is necessary to compute the system-specific parameters λ, $V_{ij}(r_{ij})$, andΔE_{ij}. We will now present details of the computation of each of these parameters.

2.4. Reorganization Energy, λ. The reorganization energy reflects the geometry relaxation in the two monomers involved in a charge transfer when their electronic state changes. In the case of hole transport, the reorganization energy is determined by four energies, (the Nelson four-point method):[31,32]

$$\lambda = E_+^* - E_+ + E^* - E \tag{5}$$

where E_+ and E are the optimized energies of the cationic and neutral forms of a single monomer, E_+^* is the energy of the monomer cation at the neutral geometry, and E^* is the energy of the neutral monomer at the cation geometry.[19−21,31,32] These energies were obtained from standard quantum chemical electronic structure calculations on a single monomer.

Monomer chemical structures of the materials studied in this paper are shown in Figure 1. Initial structures were fully optimized to obtain the reorganization energy. The cationic and neutral forms of each structure were fully optimized to obtain E_+ and E. E_+^* and E^* were obtained using single point energy calculations on the optimized neutral and cationic structures. Optimization was initially performed at the AM1 level [33] and then at the B3LYP/6-31G(d) level of theory.[34−39] This two-step optimization procedure is primarily to reduce overall computational expense,[11,40] but it also yields reorganization energies at both the AM1 and DFT levels of theory. These were both tested for use in computing mobility. An unrestricted model was used for the optimized structure in the cationic state. Some spin contamination was observed at the AM1 level, but spin contamination was typically negligible at the DFT level. All electronic structure calculations were carried out with the GAMESS program.[41]

2.5. Coupling Matrix Element, $V_{ij}(r_{ij})$. The coupling matrix element is dictated by overlap of molecular orbitals and is strongly dependent upon the relative position and orientation

of the neighboring molecules.[5,10,11,19−21,42] Several methods are in common use for determining the coupling matrix element. These have been previously been compared in detail[21,30] and will therefore only be reviewed briefly here.

2.5.1. Dimer Splitting. A common approach is the dimer splitting method, where V_{ij} is expressed as

$$V_{ij} = \frac{1}{2}\sqrt{(E_{HOMO} - E_{HOMO-1})^2 - (\varepsilon_i - \varepsilon_j)^2} \quad (6)$$

where E_{HOMO} and $E_{\mathrm{HOMO^{-1}}}$ are energies of the highest occupied and the second highest occupied molecular orbitals (HOMO and HOMO-1) of the optimized dimer structure, respectively, and $\varepsilon_i(\varepsilon_j)$ is energy of site $i(j)$. Note that these energies always appear as a difference, the difference in energy between the two molecules that results from their unique positions within the material. This difference arises not only from the differing degree to which the two monomers in an asymmetric dimer polarize each other but also from polarization of the surrounding molecules. This latter intermolecular effect is neglected in the present work. Considerable discourse on site energies may be found in the appendix of refs 20 and 43. We summarize a few essential points here: The approximation of using dimer splitting is simple to apply in an ideal system but encounters problems for complex real systems.[21,44] In an ideal system, the HOMO and HOMO-1 of the dimer are formed from a linear combination of the HOMOs of the two isolated monomers, but in a complex real system, there are many energetically closely placed orbitals, and it is difficult to identify the pair of split orbitals in the dimer that originate from the monomer HOMOs. Often there is sufficient mixing that no such pair exists. Detailed discussion of this matter may be found in ref 21.

In a crystal, the site energy difference term in eq 6 often vanishes because every molecule is equivalent in the crystal, feels an identical chemical environment, and is therefore polarized identically. When the interacting monomers are not symmetry related, however, each molecule has different chemicophysical interactions, inducing a different degree of polarization in its surroundings when charged, and the site energy difference is not zero.[11,21,42] The coupling matrix element in these asymmetric systems has been investigated by Valeev et al., who showed that the coupling matrix element in a noncofacially stacked dimer should consider the site energy correction because the monomers polarize each other differently.[42]

One approximate method to estimate the site energy difference in the calculation of the coupling matrix element is to use the HOMO level of each isolated molecule in dimer for its site energy. This approach neglects the influence of the matrix surrounding the dimer, which we will show below is a severe approximation.

2.5.2. Semiempirical Approximation to the Coupling Matrix Element. Another way to estimate the coupling matrix element, which skirts the site energy problem, is to use a semiempirical approach. A few different methods have been introduced.[45] We tested one of the most common approximations, which assumes

$$V = 1.75 S_{ij} \frac{(E_i + E_j)}{2} \quad (7)$$

Here, E_i and E_j are HOMO energies of the two isolated monomers, and S_{ij} is the overlap integral between the orbitals of the isolated monomer in the dimer geometry, $\langle\phi_i|\phi_j\rangle$. In this approximation, the coupling matrix element strongly depends on the relative orientation of the monomers within the dimer. The principal disadvantages of the semiempirical approximation are that it invokes an empirical parameter (1.75) and neglects the effect of the matrix surrounding the dimer.

2.5.3. Fock Transfer Integral. Within a one-electron product description of the electronic structure, a more rigorous way to determine the coupling matrix element that also avoids the issue of site energy difference is by direct computation of the Fock transfer integral (FTI).[21,44,46−53] Several direct calculation methods have been investigated.[21,44,46−53] Troisi and Orlandi used the FTI to calculate the coupling matrix element in DNA and obtained satisfactory results in comparison with experiments.[44] In their method, the coupling matrix element is written as

$$V = \langle \varphi_{a,HOMO} | F_{ab} | \varphi_{b,HOMO} \rangle \quad (8)$$

where F is the Kohn−Sham−Fock matrix for the dimer and ϕ_{HOMO} is approximated by Löwdin orthogonalization of monomer HOMO orbitals. After orthogonalization through terms of second order, the coupling matrix element is given by

$$\begin{aligned} V &= \langle \varphi_a' | F | \varphi_b' \rangle \\ &= (\langle \varphi_a | \alpha + \langle \varphi_b | \beta) | F | (\alpha | \varphi_b \rangle + \beta | \varphi_a \rangle) \\ &= \alpha\beta \langle \varphi_a | F | \varphi_a \rangle + \alpha^2 \langle \varphi_a | F | \varphi_b \rangle + \beta^2 \langle \varphi_b | F | \varphi_a \rangle \\ &\quad + \alpha\beta \langle \varphi_b | F | \varphi_b \rangle \end{aligned} \quad (9)$$

where $\alpha = 1 + 3/8S^2$ and $\beta = -1/2S$, and S is the overlap integral of the monomer HOMOs in the dimer geometry.[21]

We calculated the coupling matrix element using all three different techniques: dimer splitting (with and without use of the monomer HOMO energies to approximate the site energies), semiempirical method given by eq 7,[45] and direct calculation of the FTI as given by eq 9.[21] For the two acenes, the coupling matrix element was only calculated by dimer splitting and direct calculation of the FTI because the site energy difference vanishes for equivalent sites in the crystalline acenes. Finally, as detailed below, the FTI was selected for use in the present work.

2.6. Site Energies. Even when the coupling matrix element (V_{ij}) is computed by the FTI method, it is necessary to compute the site energy difference. This is because when predicting charge mobility, the site energy correction appears in two places. One case is when the coupling matrix element is calculated by the dimer-splitting method as expressed by eq 6. The other case is for introducing the energetic disorder of the hopping sites into eq 4, i.e., to evaluate the exponential term in eq 4. We tested two approaches for approximating the site energy difference. In the first approach, the HOMO level of each isolated monomer in the dimer geometry is taken as its site energy. The second approach is to approximate the site energy with an empirical potential. This potential is taken to be a sum of three separate potentials: Coulombic, non-Coulombic intermolecular, and intramolecular interaction.[10,54−57]

$$V_{total} = V_{Coulomb} + V_{non\text{-}Coulomb} + V_{intra} \quad (10)$$

To calculate the Coulomb interactions, the Wolf method[58] was employed

$$V_{Coulomb} = \sum_{i>j} \frac{q_i q_j}{4\pi\varepsilon\varepsilon_0} \left(\frac{erfc(\alpha r_{ij})}{r_{ij}} - \frac{erfc(\alpha r_c)}{r_c} + \left(\frac{erfc(\alpha r_c)}{r_c} + \frac{2\alpha}{\sqrt{\pi}} \frac{\exp(-\alpha^2 r_c^2)}{r_c} \right) (r_{ij} - r_c) \right) \quad (11)$$

where ε_0 is the permittivity of vacuum, ε is the dielectric constant, and q_i and q_j are the MOPAC charge for AM1 level (Mulliken charge for DFT level) at atom i and j, respectively. The dielectric constant is used as 3, which is typical of many electro-optic materials. The cutoff radius, r_c, was 12 Å, and the damping factor, α, was 0.2 $Å^{-1}$.

The non-Coulombic intermolecular interactions are given by Grimme's method,[57] which is expressed as

$$V_{non\text{-}Coulomb} = -\frac{C_6^{ij}}{r_{ij}^6}\left(\frac{1}{1 + \exp\left(-d\left(\frac{r_{ij}}{S_R R_{vdW}} - 1\right)\right)}\right) \quad (12)$$

where r_{ij} is the atom−atom separation, C_6^{ij} is dispersion coefficient, R_{vdW} is equilibrium van der Waals separation, d is damping coefficient, and S_6 is scaling factor for R_{vdW}. The geometric mean and simple average combination rules were employed for C_6^{ij} and R_{vdW}, respectively:

$$C_6^{ij} = \sqrt{C_6^i C_6^j}, \qquad R_{vdW} = \frac{R_i + R_j}{2} \quad (13)$$

The dispersion coefficients and the van der Waals radii for the different atoms were obtained from Grimme's publication,[57] and d and S_r were set as 1 and 0.5, respectively.

The intramolecular interactions were employed by the amber-type force field as

$$V_{intra} = \sum_{bonds} K_r(r - r_{eq})^2 + \sum_{angles} K_\theta(\theta - \theta_{eq})^2 + \sum_{dihedrals} K_\varphi(1 - \cos(\varphi - \varphi_{eq})) \quad (14)$$

Where r_{eq}, θ_{eq}, and ϕ_{eq} are determined by the optimized structures. We set K_r = 400 kcal/mol $Å^2$, K_θ = 70 kcal/mol radian^2, and K_ϕ = 30 kcal.[56]

3. CONVERGENCE TESTS

The charge mobility in molecular materials as approximated by Marcus−Hush theory depends on the reorganization energy and the coupling matrix element. These two parameters can be calculated by using electronic structure methods. In principle, any of the quantum electronic structure methods in the toolkit of computational chemistry can be applied to compute these quantities, but in practice, we require a computationally efficient approach. This is especially true for computing the coupling matrix element because of the large number of such computations involved in predicting hole mobility based on an ensemble of amorphous cells. Two approaches are reported here: First, both the reorganization energy and the coupling matrix elements were computed with the semiempirical AM1 method. Since many fewer calculations of the reorganization energy are required than calculations of the coupling matrix element, it is reasonable to apply more advanced methodology for the computation of reorganization energy. In the second approach, the reorganizations energy is computed at the DFT/B3LYP/6-31G(d)[34−39] level, and the coupling matrix elements are computed at the AM1[33] level. The second approach has proven successful in the past[20,21] and is termed the "hybrid" method. Using these approaches, we performed numerous convergence tests to identify an appropriate set of assumptions.

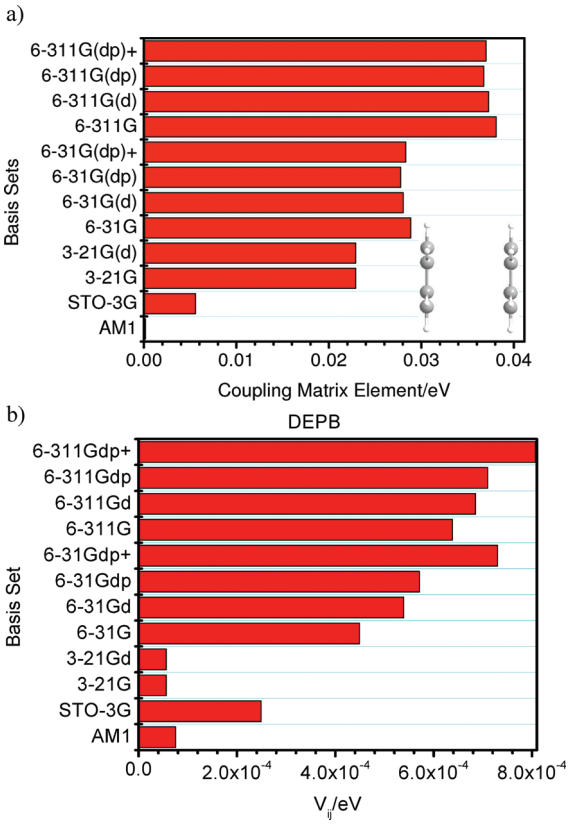

Figure 3. Coupling matrix element dependence on basis set as calculated by the FTI method: (a) parallel naphthalene and (b) DEPB dimers.

3.1. Basis Set Selection. To study the influence of basis set change, we calculated the coupling matrix element in the parallel naphthalene dimer and a DEPB dimer as well as the reorganization energy of mBPD using an assortment of different basis sets.

As shown in Figure 3a, the coupling matrix element (FTI method) in the naphthalene dimer is more strongly influenced by the size of the basis set than by the addition of polarized or diffuse functions. The coupling matrix element appears to be reasonably well converged at the triple-ζ level and is only about 25% too small at the double-ζ level. With a minimal basis set, and at the AM1 level,[33] (which has an implicit minimal basis) the coupling matrix element is significantly underestimated. This underestimation arises from the fact that $\pi-\pi$ overlap is significantly underestimated in a minimal basis. The parallel naphthalene dimer therefore represents an extreme case because the interaction is exclusively of the $\pi-\pi$ type. The calculated coupling matrix element is influenced by the wave function overlap between the monomers in a dimer, which depends on their relative spatial orientation.[59] Figure 3b shows the results of a similar convergence test for an asymmetric DEPB dimer. Note that while AM1 still underestimates the coupling matrix element, in this case it is too small by about a factor of 6, as compared to more than 100 in the case of the parallel naphthalene dimer.

Figure 4 shows the reorganization energy of mBPD as computed with different basis sets. The reorganization energy does not show strong basis set dependence. Consequently, the predicted mobility is not highly sensitive to the basis set used in the

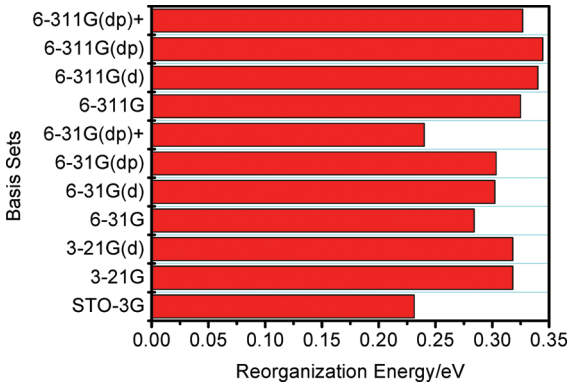

Figure 4. Reorganization energy of mBPD calculated using different basis sets.

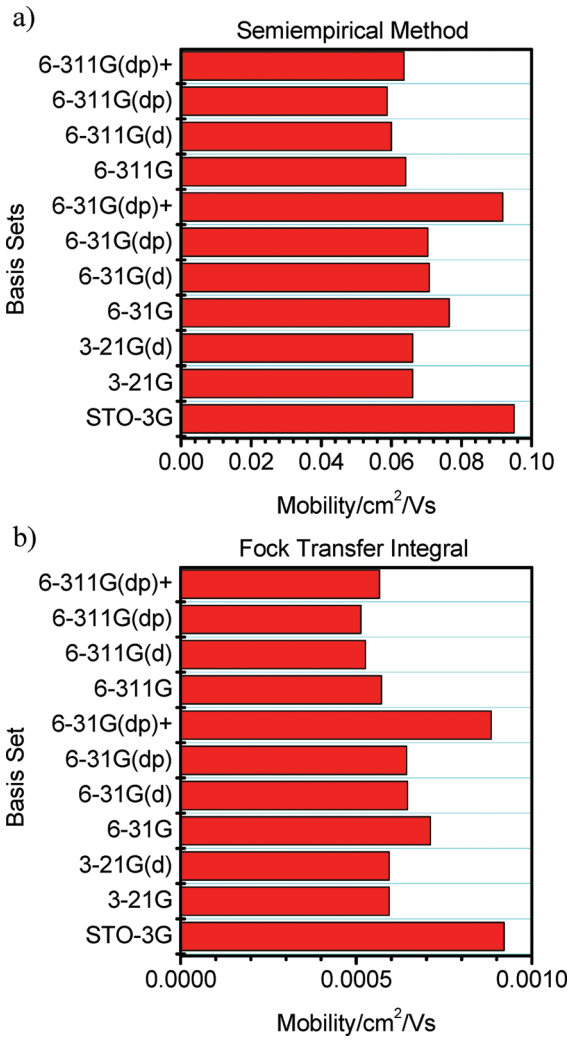

Figure 5. Dependence of predicted charge mobility of mBPD on basis set. The coupling matrix element was computed by (a) semiempirical and (b) FTI methods.

computation of λ. Even when a minimal basis set is used, λ is not grossly inaccurate.

Figure 5 shows predicted charge mobility of mBPD as computed with various basis sets. Tests were performed with the

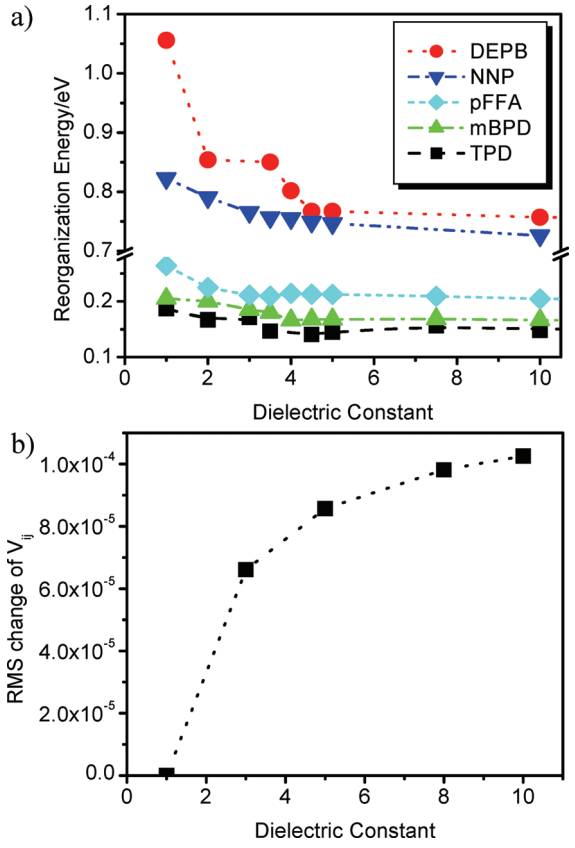

Figure 6. Dependence on dielectric constant for (a) reorganization energy and (b) coupling matrix element.

coupling matrix element calculated by the semiempirical method (Figure 5a) and by the FTI (Figure 5b). The predicted mobility does not change much with change in basis set, except with the 6-31G(dp)+[36−39] and STO-3G[60] basis sets. This is similar to the case of the reorganization energy, which similarly shows significant deviations only for these two basis sets, suggesting that the sensitivity of the predicted charge mobility to basis set is dominated by the reorganization energy. Based on the above convergence tests, the 6-31G(d)[36−39] basis set is selected for all DFT calculations as the best compromise of efficiency and completeness.

3.2. Dielectric Constant. The influence of the dielectric properties of the surrounding matrix on the reorganization energy is shown in Figure 6a. The reorganization energy decreases with increasing dielectric constant. This result demonstrates that the reorganization energy depends on the chemical environmental. For this reason, $\varepsilon = 3$ was used throughout this study, as this value is representative of many conducting organic materials.[61]

No significant dependence of the coupling matrix element on dielectric constant was found. Figure 6b shows the root-mean-square change in the computed coupling matrix element as computed with dielectric constant (ε) = 1.0 and as computed with dielectric constant set to the value given on the horizontal axis for an ensemble of 60 mPBD dimers. Note that the change is trivial, being smaller than typical values of the coupling matrix element by a factor of $\times 100$.

The reorganization energy reflects the structural relaxation that accompanies oxidation/reduction. In a high-dielectric medium, the relaxation of the molecule is restricted, so the

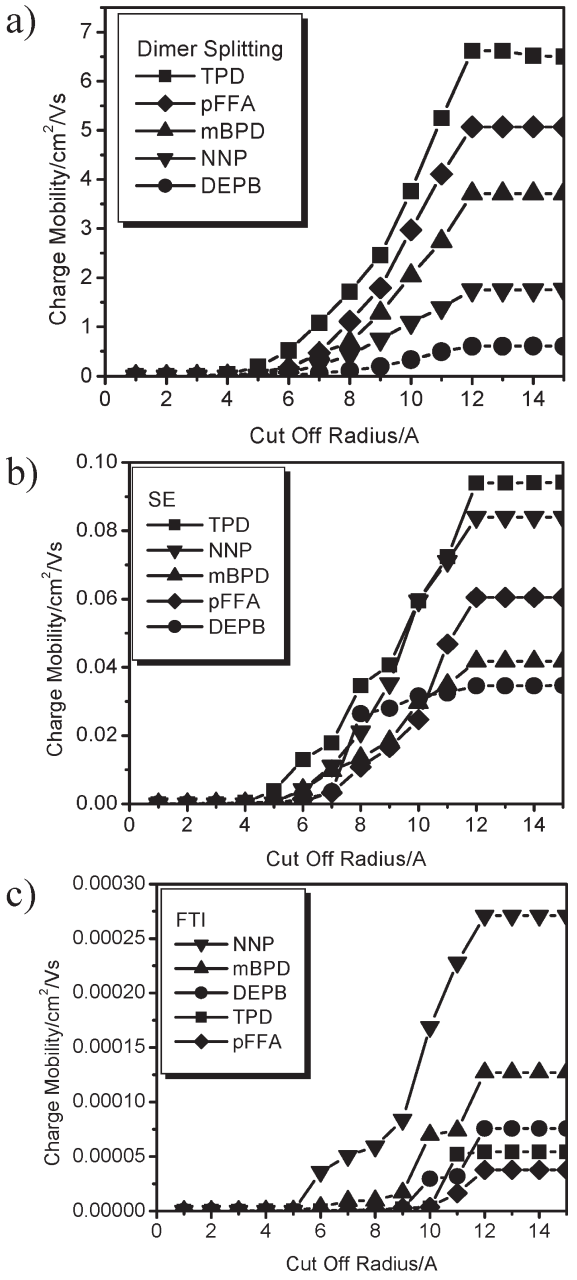

Figure 7. Dependence of predicted charge mobility on cut off radius for the five amorphous materials. B3LYP/6-31G(d) was used to compute reorganization energy and AM1 to compute coupling matrix elements by three different methods: (a) Dimer splitting method without the site energy correction was used, (b) dimer splitting method with HOMO level for the site energy was used, (c) FTI method with sum of empirical potential functions for the site energy was used.

reorganization energy gets smaller. In an amorphous material, each monomer is not equivalent because each feels different chemicophysical interactions due to spatial disorder, so the reorganization energy has to include the effect by the local environment. This is the origin of the energetic disorder of the hopping sites.

3.3. Cut-Off Radius Selection. Figure 7 shows the computed mobility in TPD as a function of the cutoff radius used in the weighted average summation of hopping rates given by eq 3. Periodic boundary conditions were employed to find the neighbors outside of the explicit unit cell. Figure 7a shows the case where V_{ij} is computed by dimer splitting. Figure 7b shows the case where V_{ij} is computed by the semiempirical method, and Figure 7c shows the case where V_{ij} is computed by FTI. In all cases the predicted mobility is converged for $R_c \geq 12$ Å, which was therefore the value used throughout the rest of the investigation.

3.4. Selection of the Method Used for Computing Coupling Matrix Element. The calculated mobility values for the five amorphous materials and two crystalline acenes wherein the coupling matrix element were computed by the dimer splitting method are shown in Figure 8 (denoted "D.S."). The mobilities of the amorphous materials are greatly overestimated but not for the acenes. We can assume that the origin of this difference lies in the two parameters: reorganization energy and coupling matrix element. In a crystal of high symmetry, the dimer splitting method is often a good way to estimate coupling matrix element, but it is not good for amorphous materials because the site energy different term in eq 6 is not small and cannot be assumed to vanish. Therefore, to predict the charge mobility in amorphous materials adequately, the site energy correction is needed.

One way to approximate the site energy is to use the HOMO level of each monomer as its site energy. The predicted charge mobility for each of the systems studied here using dimer splitting with the HOMO energy approximation for site energy is shown in Figure 8 (denoted "HOMO"). The predicted values improve over the case here where dimer splitting alone is used, but they are still greatly overestimated and show essentially no correlation to experimental values from the literature. It seems dimer splitting, with or without HOMO level approximation to the site energy, does not work well in these amorphous systems.

A method of approximating the coupling matrix element that is one step more advanced than dimer splitting is to use a semiempirical method. Here we tested a method given by eq 7. The coupling matrix element is strongly related to the relative spatial orientation of the monomers in the dimer. This semiempirical method reflects the orientational dependence of coupling matrix element because it uses the overlap integral between the monomers in the dimer geometry. The predicted charge mobilities (Figure 8, denoted "Semi") are improved over those predicted by D.S., but the values are still significantly overestimated and show weak correlation to experimental values, at best.

Using the FTI is another way to obtain the coupling matrix element that avoids the site energy difference problem.[21,44,46−53] The predicted charge mobility using the coupling matrix element as computed with FTI method is shown in Figure 8c and d. The predicted values are much improved over those obtained using the semiempirical method of calculating the coupling matrix element. When the site energy difference is neglected, however, (SP = 0) there are still some substantial disagreements with the experimental results. As discussed in Section 2.6, we tested two different methods to approximate the energetic disorder. One method is using the HOMO level of the monomer to approximate its site energy. The other method is to approximate each site's energy with an empirical potential function (denoted "EPE" in Figure 8). Agreement is better when the site energies are approximated using the empirical potential approach. The predicted charge (hole) mobilities for all of the amorphous materials are within about one order of magnitude of the experimental results. For the acenes, the predicted values are

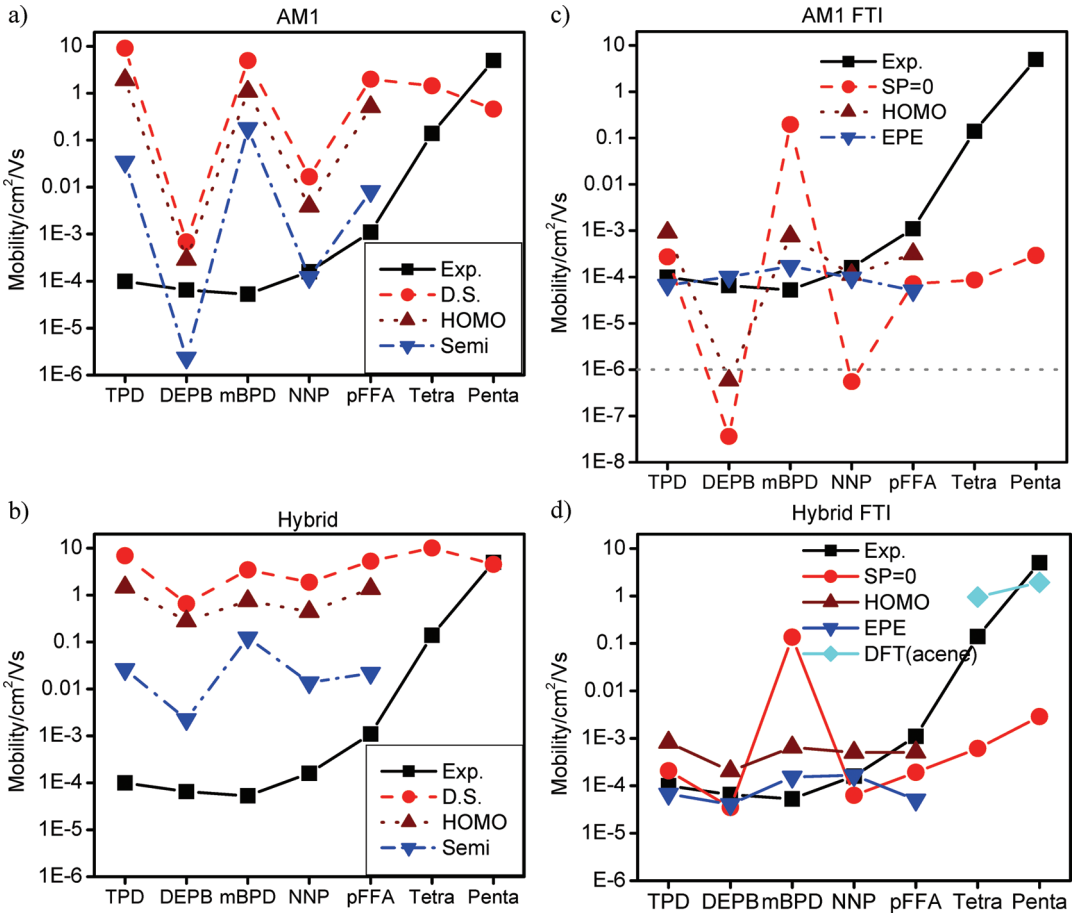

Figure 8. Predicted charge mobility for the five amorphous materials studied here: (a) using AM1 for all electronic structure calculations with the coupling matrix element calculated by three different methods: (b) using B3LYP/6-31G(d) to compute reorganization energy and AM1 to compute coupling matrix elements by three different methods; (c) using AM1 for all electronic structure calculations and three different methods to estimate the site energy difference; and (d) using B3LYP/6-31G(d) to compute reorganization energy, AM1 to compute coupling matrix elements and three different methods to estimate the site energy difference. [The dotted horizontal line depicts the lower limit of the vertical axis used in (a), (b), and (d) for comparison.] The technique marked "EPF" is the most robust approach considered here and is recommended. To obtain the DFT(acene) points, DFT was used for all electronic calculations.

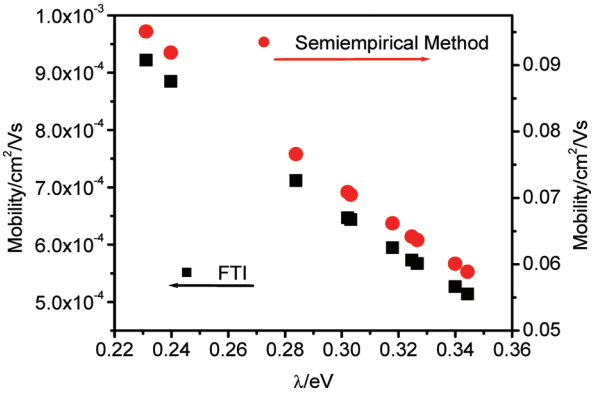

Figure 9. Charge mobility of mBPD as a function of the reorganization energy calculated using different basis sets. Black squares represent calculations where the coupling matrix element was computed with the FTI method and red circles with the semiempirical method.

severely underestimated in comparison to published experimental results. The origin of this error appears to be the small wave function overlap in the parallel dimer in the crystal of the acenes (see Figure 2). Since $\pi-\pi$ overlap is artificially low in small basis set calculations, the coupling matrix element is underestimated. When the coupling matrix elements are calculated at the DFT/B3LYP/6-31G(d)[34−39] level of theory for the crystalline acenes (this is not computationally practical for the amorphous materials), we again see order of magnitude agreement with experimental results (denoted "DFT" in Figure 8d).

To further compare the semiempirical and the FTI methods, we plot the charge mobility of mBPD as a function of the reorganization energy in Figure 9. The different values of reorganization energy result from the use of different basis sets. The calculated charge mobility linearly decreases with increasing reorganization energy. The results from the semiempirical method and the FTI show the same slope, only the scale is different. This shows that the absolute magnitude of the mobility is strongly related to the reorganization energy, but the same basic physics of the charge transport is captured in both methods of estimating the coupling matrix element. It is reasonable to surmise that the two methods will predict qualitatively similar trends and therefore will be useful for screening materials based on relative mobilities.

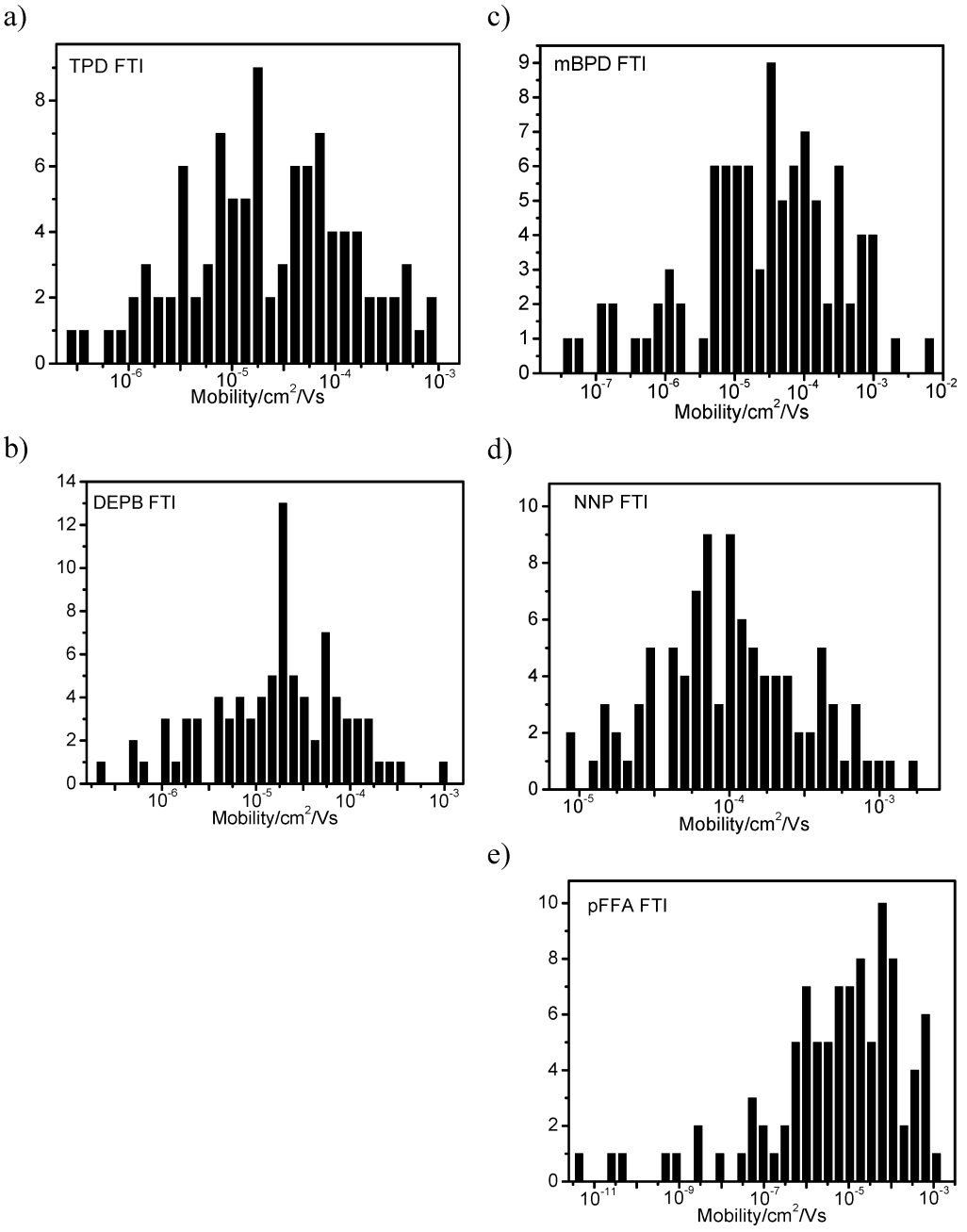

Figure 10. Histograms showing the computed hole mobilities for ensembles of ∼100 amorphous cells for each of the five systems studied here: (a) TPD, (b) DEPB, (c) mBPD, (d) NNP, and (e) pFFA.

4. DISCUSSION

Histograms based on the predicted mobilities for ∼100 amorphous cells of each of several different species considered here are presented in Figure 10. Note that the spectrum of values exhibits a clear peak in this log−scale plot. Throughout this work, the average of such an ensemble is reported as the computed mobility value. It is important to note, however, that the range of values is quite broad, typically spread over 2−3 orders of magnitude.

The calculated and (where available) experimental reorganization energy values for the species considered here are given in Table 2. The calculated values at DFT level (B3LYP/6-31G(d))[34−39] agree well with the experimental values. The experimental values of the charge mobility are also in Table 2. Two acene molecules show high charge mobility due to low reorganization energy. In amorphous materials, the charge mobility is less strongly related to the reorganization energy.

Figure 11 shows the dependence of charge mobility on material density. To evaluate this dependence, the cells were built up in two different ways. The first was by expansion of cell. In the expended cell, the individual molecules in the cell have the same relative orientation but have different center to center distances. The second approach was reconstruction of cell, wherein the new cells were developed with different size cubic parameter, so the orientations or the monomers within the cells changed. The results are essentially the same in the two cases.

Table 2. Calculated Reorganization Energy and Corresponding Experimental Data for Several Amorphous Materials as well as Crystalline Tetracene and Pentacene

		TPD	DEPB	mBPD	NNP	pFFA	tetracene	pentacene
	AM1	0.2501	1.1023	0.2706	0.8395	0.3036	0.2684	0.2740
λ/eV	DFT[1]	0.2740	0.4390	0.3022	0.3803	0.2189	0.1119	0.09349
	expt.	0.29[a]					0.1176[b]	0.0992[b]
	our work[2]	6.7×10^{-5}	4.1×10^{-5}	1.5×10^{-4}	1.7×10^{-4}	5.1×10^{-5}	0.95	1.9
mobility, cm^2/V s	expt.	$\sim 10^{-4}$,[c]	$5-8 \times 10^{-5}$,[c]	5.3×10^{-5},[d]	1.6×10^{-4},[d]	1.1×10^{-3},[e]	0.14,[f]	3,[h]
							0.4[g]	5∼7[i]

[1] DFT values were calculated at B3LYP/6-31G(d) theory level using GAMESS.[34−39,41] [2] Hybrid method was adopted for amorphous material and DFT for acenes. V_{ij} was calculated by FTI method. [a] Refs 62 and 63 [b] Refs 64 and 65 [c] Ref 66. [d] Ref 67. [e] Ref 68. [f] Ref 69. [g] Ref 70. [h] Ref 71. [i] Ref 72.

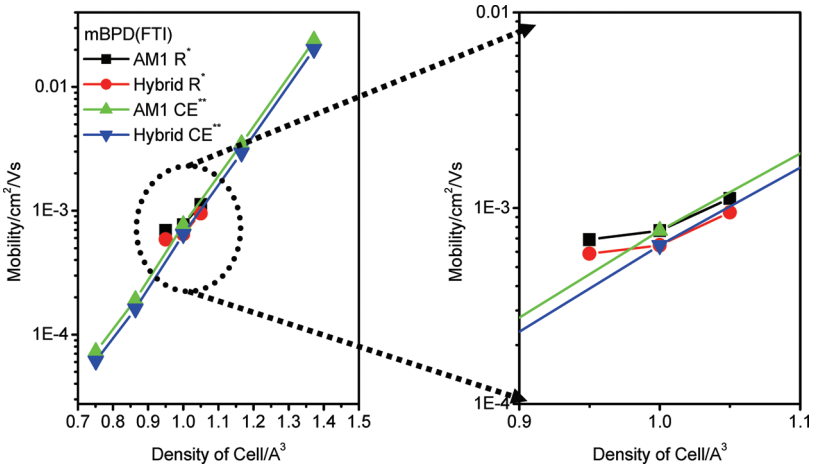

Figure 11. Predicted charge mobility of mBPD as a function of cell density; * indicates complete reconstruction of the cell and ** indicates simple cell expansion.

The charge mobility is exponentially increased with cell density, because the coupling matrix element strongly depends on wave function overlap and decreases exponentially with increasing center to center distance. Reliable estimation of material density is therefore critical for the accurate prediction of hole mobility in amorphous organic materials.

According to eqs 1−3, the charge-hopping rate depends exponentially on the reorganization energy and quadratically on the coupling matrix element. In consulting the above results, it is clear that for the amorphous materials, the charge mobility depends linearly on the reorganization energy and exponentially on the coupling matrix element. Since these two parameters, the reorganization energy and the coupling matrix element, influence the charge mobility, to improve the charge mobility of a material, those two parameters need to be controlled. The reorganization energy cannot be changed without altering the molecule. In our previous work[11] on phthalocyanine, we showed that the coupling matrix dominates charge mobility. In a strong conjugated system, like phthalocyanine and many other discotic molecules, the charge mobility depends more strongly on the coupling matrix element than on the reorganization energy.[7] This arises because the system is not changed much during the redox process because of the presence of the strong resonance structure, so the reorganization is small. In an amorphous material, therefore, changing the orientation (changing the coupling matrix element) is a better way to control the charge mobility.

To study the relation between the predicted charge mobility and the material density, we plotted the predicted charge mobility as a function of the number of carbons in unit volume, as shown in Figure 12. There is a strong relation between the two parameters. The predicted mobility increases exponentially with the carbon density. This result is similar to the relation of the mobility and the cell density of mBPD shown in Figure 11. It again follows that the predicted mobility depends more strongly on the coupling

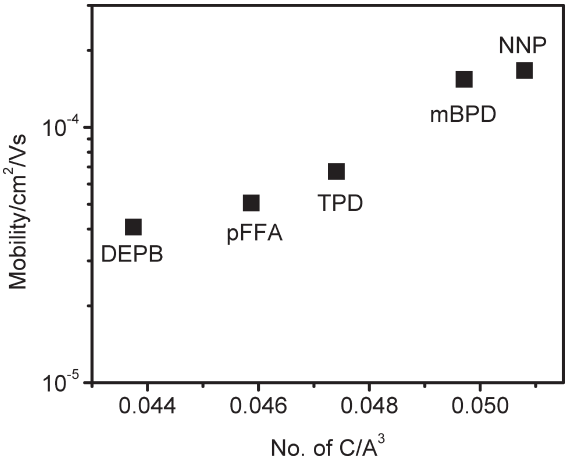

Figure 12. Predicted charge mobility of the amorphous materials as a function of number of carbon atoms in a unit volume. The coupling matrix element was calculated by the FTI method, and the site energy was estimated with an empirical potential (eq 10).

matrix than on the reorganization energy in the amorphous molecules. This result shows that to develop new material with high charge mobility, a potentially fruitful approach is to increase the density of the material.

5. CONCLUSIONS

The application of a generalization of Deng and Goddard's implementation of Marcus hopping theory to the estimation of hole mobility in amorphous organic materials has been presented here in detail. The approach is based on determining an average mobility based on an ensemble of amorphous cells representative of the material. In the most successful approach, the reorganization energy is calculated at the B3LYP/6-31G(d)[34−39] level and includes an adjustment of the dielectric constant to match that of the material. The coupling matrix elements are calculated at the AM1 level by the FTI method based on orthogonalized monomer HOMOs. The AM1 method is used for computational efficiency, since thousands of such calculations are required. The hopping site energies are approximated with an empirical potential energy function that includes Coluombic, non-Coulombic, and intramolecular interaction terms. All adjacent monomers within 12 Å of the representative central molecule are included in the calculation.

The results show that unlike crystalline organic molecular solids, charge (hole) mobility is more highly dependent on the coupling matrix elements than on the monomer reorganization energy in these amorphous organic materials that have similar reorganization energy. Furthermore, the mobility is highly sensitive to material density, showing that a reliable estimate or mobility requires accurate prediction of the material density.

It is likely that the use of the AM1 method for the computation of the coupling matrix elements underestimated their magnitude quite significantly. It would be desirable to apply more advanced electronic structure methodology in their computation, but this is impractical due to the sheer number of such calculations that are required to apply hopping theory to an ensemble of amorphous cells. This is probably the most pressing issue that needs to be addressed to improve the reliability of predictions of charge (hole) mobility in these materials. An electronic structure method that provides the reliability of a split-valence basis DFT calculation at the cost of AM1 is needed. Nevertheless, the approach outlined here appears to provide order of magnitude estimates of charge (hole) mobility in amorphous organic materials.

AUTHOR INFORMATION

Corresponding Author
*E-mail: sohlbergk@drexel.edu.

ACKNOWLEDGMENT

This research was supported by National Science Foundation grant CHE0449595 and E. I. du Pont de Nemours & Co., Inc. Thanks also to Dr. K. Dobbs for his sustained encouragement of this research.

REFERENCES

(1) Murphy, A. R.; Fréchet, J. M. J. *Chem. Rev.* **2007**, *107*, 1066.
(2) Wang, L.; Nan, F.; Yang, X.; Peng, Q.; Li, Q.; Shuai, Z. *Chem. Soc. Rev.* **2010**, *39*, 423.
(3) Kumar, A.; Liao, H.-H.; Yang, Y. *Org. Electron.* **2009**, *10*, 1615.
(4) Dimitrakopoulos, C. D.; Mascaro, D. J. *IBM J. Res. Dev.* **2001**, *45*, 11.
(5) Tant, J.; Geerts, Y. H.; Lehmann, M.; Cupere, V. D.; Zucchi, G.; Laursen, B. W.; Bjørnholm, T.; Lemaur, V.; Marcq, V.; Burquel, A.; Hennebicq, E.; Gardebien, F.; Viville, P.; Beljonne, D.; Lazzaroni, R.; Cornil, J. *J. Phys. Chem. B* **2005**, *109*, 20315.
(6) Laschat, S.; Baro, A.; Steinke, N.; Giesselmann, F.; Hägele, C.; Scalia, G.; Judele, R.; Kapatsina, E.; Sauer, S.; Schreivogel, A.; Tosoni, M. *Angew. Chem., Int. Ed.* **2007**, *46*, 4832.
(7) Andrenko, D.; Kirkpatrick, J.; Marcon, V.; Nelson, J.; Kremer, K. *Phys. Status Solidi B* **2008**, *245*, 830.
(8) Lemaur, V.; Filho, D. A.; Da, S.; Corpceanu, V.; Lehmann, M.; Geerts, Y.; Piris, J.; Debije, M. G.; van de Craats, A. M.; Senthilkumar, K.; Siebbeles, A; Warman, L. D.; Brédas, J. M.; Cormin, J.-L. J. *J. Am. Chem. Soc.* **2004**, *126*, 3271.
(9) Crispin, X.; Cornil, J.; Friedlein, R.; Okudaira, K. K.; Lemaur, V.; Crispin, A.; Kestemont, G.; Lehmann, M.; Fahlman, M.; Lazzaroni, R.; Geerts, Y.; Wendin, G.; Ueno, N.; Brédas, J.-L.; Salaneck, W. R. *J. Am. Chem. Soc.* **2004**, *126*, 11889.
(10) Andrienko, D.; Marcon, V.; Kremer, K. *J. Chem. Phys.* **2006**, *125*, 124902.
(11) Lee, C.; Sohlberg, K. *Chem. Phys.* **2010**, *367*, 7.
(12) Tse, S. C.; Cheung, C. H.; Su, S. K. Charge transport and injection in amorphous organic semiconductors. In *Organic Electronics: Materials, Processing, Devices and Applications*; So, F., Ed.; , CRC Press: Boca Roton, FL, 2010; pp 61−109.
(13) Arkhipov, V. I.; Fishchuk, I. I.; Kadashchuk, A.; Bässler, H. Charge transport in disordered organic semiconductors. In *Photophysics of Molecular Materials: From single molecules to single crystals*; Lanzani, G. , Ed.; Wiley-CVH: Weinheim, Germany, 2006; pp 261−366.
(14) Fishchuk, I. I.; Kadashchuk, A.; Bässler, H.; Nešpůrek, S. *Phys. Rev. B* **2003**, *67*, 224303.
(15) Bässler, H.; Schweitzer, B. *Acc. Chem. Res.* **1999**, *32*, 173.
(16) Bässler, H. *Phys. Status Solidi* **1993**, *175*, 15.
(17) Tsung, K. K.; So, S. K. *Appl. Phys. Lett.* **2008**, *92*, 103315.
(18) Cheung, C. H.; Tsung, K. K.; Kwok, K. C.; So, S. K. *Appl. Phys. Lett.* **2008**, *93*, 083307.
(19) Deng, W.-Q.; Goddard, W. A. *J. Phys. Chem. B* **2004**, *108*, 8614.
(20) Rossi, M.; Sohlberg, K. *J. Phys. Chem. C* **2009**, *113*, 6821.
(21) Rossi, M.; Sohlberg, K. *J. Phys. Chem. C* **2010**, *114*, 12173.
(22) Schönherr, G.; Bässler, H. *Philos. Mag. B* **1981**, *44*, 47.
(23) Novikov, S. V.; Dunlam, D. H.; Kenkre, V. M.; Pattis, P. E.; Vannikov, A. V. *Phys. Rev. Lett.* **1998**, *81*, 4472.
(24) Nešpůrek, S.; Sworakovski, J. *Thin Solid Films* **2001**, *393*, 168.
(25) *Material Studio*; Accerlys Inc.: San Diego, CA.
(26) Rigby, D. *Fluid Phase Equilib.* **2004**, *217*, 77.
(27) Robertson, J. M.; Sinclair, V. C.; Trotter, J. *Acta Crystallogr.* **1961**, *14*, 697.
(28) Campbell, R. B.; Robertson, J. M.; Trotter, J. *Acta Crystallogr.* **1961**, *14*, 705.
(29) Marcus, R. A. *J. Chem. Phys.* **1955**, *24*, 966.
(30) Marcus, R. A.; Sutin, N. *Biochim. Biophys. Acta* **1985**, *115*, 265.
(31) Wu, Q.; Voorhis, T. V. *J. Phys. Chem. A* **2006**, *110*, 9212.
(32) Nelsen, S. F.; Blackstock, S. C.; Kim, Y. *J. Am. Chem. Soc.* **1987**, *109*, 677.
(33) Dewar, M. J. S.; Zoebisch, E. G.; Healy, E. F.; Stewart, J. J. P. *J. Am. Chem. Soc.* **1985**, *107*, 3902.
(34) Becke, A. D. *J. Chem. Phys.* **1993**, *98*, 1372.
(35) Lee, C.; Yang, W.; Parr, R. G. *Phys. Rev. B* **1988**, *37*, 785.
(36) Ditchfield, R.; Hehre, W. J.; Pople, J. A. *J. Chem. Phys.* **1971**, *54*, 724.
(37) Hehre, W. J.; Dichfield, R.; Pople, J. A. *J. Chem. Phys.* **1972**, *56*, 2257.
(38) Hariharan, P. C.; Pople, J. A. *Mol. Phys.* **1974**, *27*, 209.
(39) Gordon, M. S. *Chem. Phys. Lett.* **1980**, *76*, 163.
(40) Lee, C.; Park, S. −K.; Min, K. −C.; Kim., Y.; Lee, N. −S. *Bull. Korean Chem. Soc.* **2008**, *29*, 1951.
(41) Schmidt, M. W.; Baldridge, K. K.; Boatz, J. A.; Elbert, S. T.; Gordon, M. S.; Jensen, J. H.; Koseki, S.; Matsunaga, N.; Nguyen, K. A.;

Su, S. J.; Windus, T. L.; Dupuis, M.; Montgomery, J. A. *J. Comput. Chem.* **1993**, *14*, 1347.
(42) Valeev, E. F.; Coropceanu, V.; da S. Filho, D. A.; Salman, S.; Brédas, J.-L. *J. Am. Chem. Soc.* **2006**, *128*, 9882.
(43) Norton, J. E.; Brédas, J.-L. *J. Am. Chem. Soc.* **2008**, *130*, 12377.
(44) Troisi, A.; Orlandi, G. *Chem. Phys. Lett.* **2001**, *344*, 509.
(45) Hare, C. R.; Sleight, T. P.; Cooper, W.; Clarke, G. A. *Inorg. Chem.* **1968**, *7*, 669.
(46) Kieninger, M.; Suhai, S. *J. Comput. Chem.* **1996**, *17*, 1508.
(47) Fujita, T.; Nakai, H.; Nakatsuji, H. *J. Chem. Phys.* **1996**, *104*, 2410.
(48) Yin, S.; Yi, Y.; Li, Q.; Yu, G.; Liu, Y.; Shuai, Z. *J. Phys. Chem. A* **2006**, *110*, 7138.
(49) Orlandi, G.; Troisi, A.; Zerbetto, F. *J. Am. Chem. Soc.* **1999**, *121*, 5392.
(50) Wu, Q.; Voorhis, T. V. *J. Phys. Chem. A* **2006**, *110*, 9212.
(51) Wu, Q.; Voorhis, T. V. *J. Chem. Phys.* **2006**, *125*, 164105.
(52) Yang, X.; Li, Q.; Shuai, Z. *Nanotechnology* **2007**, *18*, 424029.
(53) Yang, X.; Wang, L.; Wang, C.; Long, W.; Shuai, Z. *Chem. Mater.* **2008**, *20*, 3205.
(54) Williams, D. E. *J. Comput. Chem.* **2001**, *22*, 1154.
(55) Nagata, Y.; Lennartz, C. *J. Chem. Phys.* **2008**, *129*, 034709.
(56) Foster, M. E.; Sohlberg, K. *J. Chem. Theory Comput.* **2010**, *6*, 2153.
(57) Grimme, S. J. *Comput. Chem.* **2006**, *27*, 1787.
(58) Wolf, D.; Keblinski, P.; Phillpot, S. R.; Eggebrecht, J. *J. Chem. Phys.* **1999**, *110*, 8254.
(59) Brédas, J.-L.; Calbert, J. P.; da Silba Filho, D. A.; Cornil, J. *Proc. Natl. Acad. Sci. U.S.A.* **2002**, *99*, 5804.
(60) Slater, J. C. *Phys. Rev.* **1930**, *36*, 57.
(61) Schildkraut, J. S.; Buettner, A. V. *J. Appl. Phys.* **1991**, *72*, 1888.
(62) Lin, B. C.; Cheng, C. P.; Lao, Z. P. M. *J. Phys. Chem. A* **2003**, *107*, 5241.
(63) Malagoli, M.; Brédas, J.-L. *Chem. Phys. Lett.* **2000**, *327*, 13.
(64) Podzov, V.; Sysoev, S. E.; Loginova, E.; Pudalov, V. M.; Gershenson, M. E. *Appl. Phys. Lett.* **2003**, *83*, 3504.
(65) Podzov, V.; Pudalov, V. M.; Gershenson, E. *Appl. Phys. Lett.* **2003**, *82*, 1739.
(66) Mori, T.; Sugimura, E.; Mizutani, T. *J. Phys. D* **1993**, *26*, 452.
(67) Shirota, Y.; Kageyama, H. *Chem. Rev.* **2007**, *107*, 953.
(68) Okumoto, K.; Shirota, Y. *Mater. Sci. Eng. B* **2001**, *85*, 135.
(69) Butko, V. Y.; Chi, X.; Ramirez, A. P. *Solid State Commun.* **2003**, *128*, 431.
(70) de Boer, R. W.; Klapwijk, T. M.; Morpurgo, A. F. *Appl. Phys. Lett.* **2003**, *83*, 4345.
(71) Klauk, H.; Halik, M.; Zschieschang, U.; Schmid, G.; Radlik, W.; Weber, W. *J. Appl. Phys.* **2002**, *92*, 5259.
(72) Kelley, T. W.; Muyres, D. V.; Baude, P. F.; Smith, T. P.; Jones, T. D. *Mater. Res. Soc. Symp. Proc.* **2003**, *771*, L651.